Visual Servoing for Constrained Planar Robots Subject to Complex Friction

Emmanuel C. Dean-León, Vicente Parra-Vega, *Member, IEEE*, and Arturo Espinosa-Romero

Abstract—The theoretical framework and the experimental validation of a new image-based position-force control for planar robots are presented in this paper. This scheme produces simultaneous convergence of the constrained visual position and the contact force between the end effector and the constraint surface. Camera, robot, and the visual jacobian parameters are considered unknown. This approach is based on a new formulation of the orthogonalization principle used in the robot force control, termed the visual orthogonalization principle. This allows, under the framework of passivity, to yield a synergetic closed-loop system that fuses accordingly camera, encoder, and the force sensor signals. Furthermore, due to the technological limitations, it can be noticed that the visual servoing contact tasks are characterized by slow motion, typically with frequent velocity reversals along the constraint surface, thus, important friction problems arise at the joints and the contact points. Therefore, visual compensation of the complex dynamic joint friction and the viscous contact friction are also studied. A Linux real-time operating-system-based experimental system is implemented to visually drive a constrained direct-drive planar robot manipulator, equipped with six-axes JR3 force sensor and a digital fixed camera, thus proving the effectiveness of the proposed scheme.

Index Terms—Dynamic friction compensation, force control, uncalibrated visual servoing.

I. INTRODUCTION

ROBOT tasks that involve the generalized sensors (sensors that measure the state of the system), and the nongeneralized sensors (measuring any other signal) impose a challenging problem in robotics due to the nonlinear dynamics of robots along with multisensor fusion and sensor redundancy problems. For instance, consider visual servoing for the constrained robot tasks, where the generalized joint encoders, the tachometers, and the generalized momentum and force sensors are implemented along with the nongeneralized charge-coupled device (CCD) camera sensors or proximity sensors as well. However, it is well known that the multisensor-based robot control approaches may offer a solution to relevant, but complex, problems in robotics, in particular, for the unstructured tasks. Moreover, since in practice physical parameters are uncertain, the robustness to parametric

Fig. 1. Visual servoing contact task.

uncertainties is an integral part in the force-position control of a robot driven by uncalibrated visual information, where the force and joint encoder signals have to be fused along with the visual information. In our case, the task under study is that of a nonredundant robot end effector that tracks a *visual* trajectory along the surface of an object while it simultaneously exerts a desired force in the normal direction of the constraint surface. The desired visual trajectory is designed using the information provided by the fixed camera (see Fig. 1). Taking into account the fact that when two rigid surfaces are in contact, friction is always present, therefore uncertainties in the friction at the joints and tangential friction at the contact point should be considered for any practical application. In addition, for these sorts of tasks there are important open problems mainly because; from the theoretical viewpoint, these systems use redundant sensors and it is not evident how to handle the sensor fusion in a complex constrained nonlinear dynamical system, let alone visual-based compensation of friction; from the experimental viewpoint, we are dealing with a multirate system where the camera, the joint encoders, and the force sensors have all very different latencies, and whose performance is also hampered by the *dynamic friction at the joints* and the *viscous contact friction*. Therefore, a theoretical constrained visual servoing scheme must be accompanied by its real-time-based experimental validation.[1] These tasks are very relevant in many robotic applications because the camera allows us to structure the environment in contact tasks, e.g., in the textile and shoes industry, as well as in cutting,

[1]Notice that the static state of the camera is not a generalized coordinate of the dynamical system, thus its slow latency is not an issue, and the system can be treated in the time domain, when generalized coordinates are sampled very fast, in comparison to its natural frequency, even though its implementation is carried out in the digital/discrete domain.

and deburring robotic-task applications. Therefore, in order to achieve a sensor-fusion-based controller, a careful and judicious analysis of the nonlinear dynamics, the sensor behavior, and the contact tasks is required. As can be seen, the robotic tasks mentioned before imply significant difficulties and stand as a robot control paradigm that surpasses the traditional schemes in robot control and sensor fusion, thus requiring new theoretical frameworks.

A. Passivity-Based Design

Despite the availability of separate control schemes of vision or force, vision force servoing has been elusive mainly because it is not evident how to deal—into a unique framework—with vision and force signals, since these two schemes in terms of passivity were considered seemingly contradictory. On one hand, it is well known that passivity is established from the torque input to the joint velocity output, and since the *contact* torque input is orthogonal to the joint velocity, apparently for the contact tasks, the contact torque input did not provide power to the passivity inequality. Thus, it was hard to handle the contact torque. This force control problem was solved by Arimoto [1] with the orthogonalization principle (OP) that provides unobtrusively a harmonious unique signal from the generalized sensors (the encoders, the tachometers, and the force sensors) that combines the position and the contact force errors. However, when the camera is introduced to design image-based desired trajectories, a nongeneralized sensor arises that measures redundantly the generalized joint position. In this case, it was difficult to deliver a *Visual Passivity* inequality, where the passivity was enforced from the joint torque input to visual-based error velocity output. This conveyed the idea that there was no sense in mixing visual servoing in force control because, previously, we did not understand that the visual position-velocity and the force-momentum signals could blend into a unique joint output error signal to establish a *Visual Passivity* inequality, essentially because the dot product of the visual-based error velocity output and the torque input is zero.

To combine visual servoing and force control into an integrated whole, and with this, enforce passivity from a torque input to the visual joint output, the *visual orthogonalization principle* (VOP) is derived. With this result in hand, we could blend both approaches into a unique position-force robot control scheme.

B. Contribution

In this paper, a new formal solution is presented for the problem of the uncalibrated image-based robot force control under the parametric uncertainties without the singularities in the camera orientation angle. It is based on the second-order sliding-mode adaptive controller driven by the *constrained image errors* that solves by first time the problem posed earlier. The underlying reason that allows us to obtain this result is the new orthogonalized image-based error manifold derived by means of the VOP that is introduced in this article. Thus, results similar to the case of the non-visual-based orthogonalization principle are obtained. The closed-loop system guarantees exponential tracking

of the position and the force trajectories subject to parametric uncertainties under the formal stability proofs. Moreover, its experimental validation is presented on a two degree of freedom (2 DOF) direct-drive manipulator, equipped with a high-end force sensor, interacting with a highly rigid surface. The control system is running on Linux-real-time application interface (RTAI) operating system. We further extend our proposal to include the visual compensation of the dynamic friction. The simplicity of the controller enhances its practical applications since the desired task is designed in image space,[2] i.e., the user defines the desired task right from the image that she or he sees,[3] wherein a fixed camera supplies a perspective of the desired task (see Fig. 1).

C. Organization

Section II provides a review on several aspects of visual position-force robot control, while Section III introduces the nonlinear differential algebraic equations of robot dynamics in the error coordinates. Section IV presents a well-known camera-robot model, while Section V proposes the VOP, and the open-loop error equation is given in Section VI. Section VII presents the control design without friction, while the joint dynamic friction and the viscous contact friction compensation are given in Section VIII. Experimental validation is presented in Section IX, and finally conclusions are stated in Section X.

II. PREVIOUS WORKS

A variety of sensor fusion schemes for robot manipulators have been proposed recently. Some of the most important works in the related areas of visual servoing and force control are the following.

A. Visual Servoing

Visual servoing for free motion has been the subject of research for four decades. So far, a few visual-servo controllers have been proposed that take into account the nonlinear robot dynamics. However, some of them model the vision system as a simple rotation matrix [2], while some others proposed a variety of techniques for off-line camera calibration [3]. Thus, only a few approaches were aimed at the more important problem of the on-line calibration under the closed-loop control. Specifically, for the *fixed camera* configuration, [4] considered a more representative model of the camera-robot system (than previous works [2]) to design a control law for regulation task that compensates for the unknown intrinsic camera parameters, but requires exact knowledge of the camera orientation. Later, [5] presents a redesigned control law that also takes into account the uncertainties in the camera orientation and produces local asymptotic stability results, but requires the perfect knowledge

---

[2]In this paper, we refer to the image space as the numerical representation of the image captured by the camera that is stored on the computer memory as a matrix. The origin of the image space corresponds to the first element of the matrix, which also corresponds to the upper-left corner of a computer monitor when imaged.

[3]Provided that the fixed position of the camera is set to cover the robot workspace, in this way a task free of singularities can be designed.

of the robot gravitational term wherein the error of the estimation of the camera orientation is restricted to $[-90°, 90°]$. In [3], a position tracking control scheme is developed with the online adaptive camera calibration that guarantees the global asymptotic position tracking under the persistent excitation condition. Recently, in [6], an adaptive camera calibration control law that compensates for the uncertain robot-camera parameters with the global *asymptotic* position tracking is presented. Finally, [8] presents a control law that deals with the image-based compensation of the joint dynamic friction on the uncalibrated robot-camera systems. Additionally, it does not present any limitation on camera orientation (in comparison to the approaches considered earlier). Despite the availability of approaches mentioned before, none of them use the contact force information for an image-based tracking of a constrained robot system that still had remained as an open problem.

B. Force Control

Even when several methodologies have been proposed in the robot force control area, the work that provides important bases for the development of this area can be found in the pioneer articles [1], [9]–[12], which introduced the simultaneous control of position and force, using the full nonlinear dynamics subject to the parametric uncertainties with and without coordinate partitioning. However, the work [1] provided the orthogonalization principle that allows us to build a unique error signal based on the physical principle that the joint velocity arises orthogonal to the contact force. This helped establish the guidelines for the powerful passivity-based force control, with some advantages over the other approaches such as the adaptation to parametric uncertainties, the robustness for a class of bounded unmodeled dynamics, and even the exponential and the global stability. Afterwards, several schemes were proposed using these ideas; however the orthogonalization principle has not been extended, or combined, beyond the joint control of the constrained robots.

C. Visual Force Servoing

Few approaches focus on the hybrid vision/force control [13], [14]. Also, these works are not robust to the uncertainties on the robot and the camera parameters. In a different path, [15] presents an adaptive robot controller to achieve the contact tasks in an unknown environment, but this scheme requires exact knowledge of the kinematic mapping. Along similar developments, [16] introduces an interesting but inconvenient computed torque scheme for an uncalibrated environment, but their approach does not deal with the uncertainties of the robot parameters. None of the approaches mentioned before fully satisfy the statement of the problem.

D. Visual Friction Compensation

It is quite important to compensate friction because it is a dominant dynamical force in the slow motion and the velocity-reversal regimes, which are *typical* in the visual servoing tasks, let alone the contact tasks. Nevertheless, in general, the joint dynamic and the contact frictions are usually neglected in motion control, and unfortunately, it is not the exception in the visual servoing literature. To consider the joint friction compensation in a visual servoing scheme, the *LuGre* model [17] is implemented, which reproduces the presliding regime at very small displacements and hard nonlinearities, including the limit cycles. The problem becomes more complicated as even though the dynamic joint friction depends on the joint coordinates, in the image-based control the contact friction will depend on the image coordinates. Therefore, it requires a *visual compensator for the joint and the contact friction*. No previous reference to this topic is available thus far. Finally, we point out that for compensation of the friction in an image-based visual servoing task, the friction compensation algorithm should be image-based, otherwise it will be prone to instability from the uncertainties of the camera parameters.

III. NONLINEAR ROBOT DYNAMICS

The constrained robot dynamics arises when its end effector is in contact with an infinitely rigid surface. Based on [1] and including the friction dynamics, this system can be modeled by the nonlinear differential algebraic equations as follows:

$$H(q)\ddot{q} + C(q,\dot{q}) + g(q) = \tau - J_{\varphi+}^T(q)\lambda - F(\dot{q},\dot{\omega},\omega)$$
$$- J^T(q)B_t J(q)\dot{q} \quad (1)$$
$$\varphi(q) = 0 \quad (2)$$

In this paper, a fixed camera configuration is considered, where the camera plane is parallel to the robot workspace. Since a nonredundant robot manipulator is assumed, then the generalized joint position and the joint velocity coordinates are denoted by $q \in \Re^2$ and $\dot{q} \in \Re^2$, respectively, i.e., a 2 DOF robot manipulator. Matrix $H(q) \in \Re^{2\times2}$ stands for the robot inertia matrix, $C(q,\dot{q}) \in \Re^{2\times2}$ stands for the vector of the centripetal and the Coriolis torques, $g(q) \in \Re^2$ is the vector of the gravitational torques, $F(\dot{q},\dot{\omega},\omega) \in \Re^2$ is the dynamic friction,[4] $B_t \in \Re_+^{2\times2}$, is the viscous friction matrix, possibly not a diagonal matrix, $J^T(q)B_t J(q)\dot{q} \in \Re^2$ represents the tangential viscous friction at the contact point, $J_{\varphi+}^T(q) = \frac{J_\varphi^T(q)}{J_\varphi(q)J_\varphi^T(q)} \in \Re^{2\times m}$ is the constrained normalized jacobian of the kinematic constraint $\varphi(q) = 0$, or a rigid surface with a continuous gradient, and $\lambda \in \Re^m$ is the contact force, for a single contact point $m = 1$, and finally $\tau \in \Re^2$ stands for the vector of the joint torque control.

Two important properties of the robot dynamics, useful for stability analysis, are the following:

Property I: With a proper definition of $C(q,\dot{q})$ [2], $\dot{H}(q) - 2C(q,\dot{q})$ is skew-symmetric. Then

$$X^T[\dot{H}(q) - 2C(q,\dot{q})]X = 0 \quad \forall X \in \Re^2. \quad (3)$$

Property II: Robot dynamics are linearly parameterizable in terms of a known regressor $Y = Y(q,\dot{q},\ddot{q}) \in \Re^{2\times p}$ and an

---

[4]For a clear exposition, firstly, we developed the controller without the dynamic joint friction $F(\dot{q},\dot{\omega},\omega) = 0$; afterwards, Section VIII deals with $F(\dot{q},\dot{\omega},\omega)$.

unknown vector $\theta_b \in \Re^p$ of robot parameters as follows:

$$H(q)\ddot{q} + C(q,\dot{q})\dot{q} + g(q) + J^T(q)B_t J(q)\dot{q} = Y\theta_b \qquad (4)$$

Adding and subtracting the linear parameterization equation (4) to (1), produces the open-loop error equation

$$H(q)\dot{S}_q = -C(q,\dot{q})S_q - J^T(q)B_t J(q)S_q$$
$$+ \tau + J_{\varphi+}^T(q)\lambda - Y_r\theta_b$$

with joint error surface S_q defined as

$$S_q = \dot{q} - \dot{q}_r \qquad (5)$$

where $\dot{q}_r$ represents the nominal reference of joint velocities.

IV. CAMERA-ROBOT MODEL

Monocular visual servoing is considered, where both the image plane and the robot workspace are parallel; this is important since the transformation that produces the image captured by the camera is a similarity; i.e., ratios of lengths and angles are preserved, thus both the robot workspace and the desired visual task are defined in $\Re^2$. In order to design a proper *nominal reference* of the joint velocities $\dot{q}_r$, the direct and the inverse robot kinematics, as well as a static pinhole camera model are used.

Let robot direct kinematics be

$$x_b = f(q) \qquad (6)$$

where $x_b \in \Re^2$ represents the two-dimensional position of robot end effector in the robot workspace and $f(\cdot) : \Re^2 \to \Re^2$. The differential kinematics of the robot manipulator is then defined as follows:

$$\dot{x}_b = J(q)\dot{q} \qquad (7)$$

which relates the Cartesian velocities $\dot{x}_b \in \Re^2$ to joint space velocities $\dot{q} \in \Re^2$. The visual position $x_v = [u,v]^T \in \Re^2$ of the robot end effector in image space[5] is given as in [18]

$$x_v = \alpha h(z)R(\theta_v)x_b + \beta \qquad (8)$$

where $\alpha = \text{diag}[\alpha_u, \alpha_v] \in \Re_+^{2\times2}$ is the scale factor; $h(z) = \frac{\lambda_v}{\lambda_v - z} < 0, z \gg \lambda_v$, where λ_v is known as the focal distance and z is the depth of the field, θ_v is the rotation angle over the optical axis, i.e., the z axis (see Fig. 1), and $R(\theta_v) \in SO(2)$ is the upper 2×2 matrix of $R_3(\theta_v) \in SO(3); \beta \in \Re^2$, which depends on the intrinsic and extrinsic camera parameters.[6] In this way, the differential camera model becomes

$$\dot{x}_v = \alpha h(z)R(\theta_v)\dot{x}_b \qquad (9)$$

where $\dot{x}_v \in \Re^2$ determines the visual robot end-effector velocity, i.e., the *visual flow*. Notice that the constant transformation $\alpha h(z)R(\theta_v)$ maps statically robot *Cartesian velocities* $\dot{x}_b$ into the *visual flow* $\dot{x}_v$. Using (7), (9) becomes

$$\dot{x}_v = \alpha h(z)R(\theta_v)J(q)\dot{q} \qquad (10)$$

which relates the *visual flow* $\dot{x}_v$ to the *joint velocity vector* $\dot{q}$. Thus, the inverse differential kinematics of (10), in terms of the visual velocities,[7] becomes

$$\dot{q} = J_{R\text{inv}}\dot{x}_v \qquad (11)$$

where $J_{R\text{inv}} = J(q)^{-1}R(\theta_v)^{-1}h(z)^{-1}\alpha^{-1}$. This relation is useful for designing the nominal reference of the joint velocities $\dot{q}_r$ based on the VOP that we describe in Section V.

V. VOP

According to (2)

$$\frac{d}{dt}\varphi(q) = 0 \to \frac{\partial\varphi(q)}{\partial q}\frac{dq}{dt} = 0 \Rightarrow J_\varphi(q)\dot{q} \equiv 0.$$

This means that $J_\varphi(q)$ is orthogonal to $\dot{q}$, i.e., $\dot{q}$ lies in the span of the orthogonal projection Q of $J_\varphi(q)$, which arises on the tangent space at the contact point between the end effector and the surface $\varphi(q) = 0$ [1]. Thus, $Q = I - J_{\varphi+}^T(q)J_\varphi(q)$ from which we obtain that $QQ\dot{q} = Q\dot{q} \equiv \dot{q}$. As can be seen, $QJ_\varphi^T(q) = 0$. From the above implications, (11) becomes

$$\dot{q} = QJ_{R\text{inv}}\dot{x}_v. \qquad (12)$$

Naturally (12) leads us to propose the nominal reference of the joint velocity $\dot{q}_r$ in terms of the visual and the force references as follows:

$$\dot{q}_r = QJ_{R\text{inv}}\dot{x}_r + \Gamma_{F_2}J_\varphi^T(q)\dot{q}_{rf} \qquad (13)$$

where

$$\dot{x}_r = \dot{x}_{vd} - \Psi\Delta x_v + S_{vd} - \Gamma_{v_1}\int_{t_0}^t S_{v\delta}(\zeta)d\zeta$$
$$- \Gamma_{v_2}\int_{t_0}^t \text{sign}[S_{v\delta}(\zeta)]d\zeta \qquad (14)$$

$$S_{v\delta} = \underbrace{(\Delta\dot{x}_v + \Psi\Delta x_v)}_{S_v} - \underbrace{S_v(t_0)e^{-\kappa_v t}}_{s_{vd}} \qquad (15)$$

$$\dot{q}_{rf} = \Delta F - S_{Fd} + \Gamma_{F_1}\int_{t_0}^t S_{F\delta}(\zeta)d\zeta$$
$$+ \Gamma_{F_2}\int_{t_0}^t \text{sign}[S_{F\delta}(\zeta)]d\zeta \qquad (16)$$

$$S_{F\delta} = \underbrace{\Delta F}_{S_F} - \underbrace{S_F(t_0)e^{-\kappa_F t}}_{S_{Fd}} \qquad (17)$$

$$\Delta F = \int_{t_0}^t \Delta\lambda(\zeta)\,d\zeta, \quad \Delta\lambda = \lambda - \lambda_d \qquad (18)$$

where $\dot{x}_{vd}$ stands for the desired visual velocity trajectory; $\Delta x_v = x_v - x_{vd}$ is the visual position error, $\Psi = \Psi^T \in \Re_+^{2\times2}; \Delta\dot{x}_v = \dot{x}_v - \dot{x}_{vd}$ defines the visual velocity error; $\kappa_v > 0; \Gamma_{v_i} = \Gamma_{v_i}^T \in \Re_+^{2\times2}, i = 1,2$ with $\Delta\lambda$ as the force tracking error and λ_d as the desired contact force; $\kappa_F > 0$, and $\Gamma_{F_i} = \Gamma_{F_i}^T \in \Re_+, i = 1,2$. Notice that $\dot{x}_r$ is the *nominal visual reference*, $\dot{q}_{rf}$ is the *nominal force reference*, $S_{v\delta}$ is the

---

[5]The subscript "v" of x_v denotes *visual* from *visual servoing* notation.

[6]Focal distance, the depth of the field, the translation of the camera center to the image center, and the distance between the optical axis to the robot base.

[7]With $J_{R\text{inv}} \in \Re^{2\times2}$, i.e., a function of the robot and the camera parameters.

visual error surface, and $S_{F\delta}$ is the *force error surface*. Using (12)–(16) into (5), the *joint error surface* S_q is

$$S_q = QJ_{R\text{inv}}\dot{x}_v - QJ_{R\text{inv}}\dot{x}_r - \Gamma_{F_2}J_\varphi^T(q)\dot{q}_{rf}$$
$$= QJ_{R\text{inv}}S_{vv} - \Gamma_{F_2}J_\varphi^T(q)S_{vF} \qquad (19)$$

with

$$S_{vv} = S_{v\delta} + \Gamma_{v_1}\int_{t_0}^t S_{v\delta}(\zeta)d\zeta + \Gamma_{v_2}\int_{t_0}^t \text{sign}[S_{v\delta}(\zeta)]d\zeta$$

$$S_{vF} = S_{F\delta} + \Gamma_{F_1}\int_{t_0}^t S_{F\delta}(\zeta)d\zeta + \Gamma_{F_2}\int_{t_0}^t \text{sign}[S_{F\delta}(\zeta)]d\zeta$$

where S_{vv} represents the *extended visual manifold* and S_{vF} stands for the *extended force manifold*.

Remark 1: Notice that S_q is composed of two orthogonal complements, $QJ_{R\text{inv}}S_{vv}$ that depends on the image coordinate error, and $\Gamma_{F_2}J_\varphi^T(q)S_{vF}$ that depends on the integral of contact force errors. Since tracking errors $(\Delta x_v, \Delta\dot{x}_v)$ and ΔF are mapped into the orthogonal complements, they can be controlled independently.

Remark 2: The above definition assumes exact knowledge of $J_{R\text{inv}}$, i.e., *calibrated camera*. However, in practice, it stands as a very restricted assumption. Therefore, in Section IV-A, the uncalibrated camera case is considered, which gives rise to the uncertain manifold $\hat{S}_q$ that takes into consideration the uncertainty of $J_{R\text{inv}}$.

A. Uncalibrated Camera

Consider that $\alpha h(z)$ and θ_v are unknown, then (13) becomes

$$\hat{\dot{q}}_r = Q\widehat{J_{R\text{inv}}}\dot{x}_r - \Gamma_{F_2}J_\varphi^T(q)\dot{q}_{rf} \qquad (20)$$

with $\widehat{J_{R\text{inv}}}$ as an estimation of $J_{R\text{inv}}$, such that $\widehat{J_{R\text{inv}}}$ is full rank $\forall q \in \Omega_q$, where the robot workspace free of the singularities is defined by $\Omega_q = \{q|\text{rank}(J(q)) = 2, \forall q \in \Re^2\}$. Thus, using (20) into (5), we have the *uncalibrated joint error surface*

$$\hat{S}_q = \dot{q} - \hat{\dot{q}}_r$$
$$= QJ_{R\text{inv}}\dot{x}_v - Q\widehat{J_{R\text{inv}}}\dot{x}_r - \Gamma_{F_2}J_\varphi^T(q)\dot{q}_{rf} \qquad (21)$$

where $\hat{S}_q$ is available because $\dot{q}$ and $\hat{\dot{q}}_r$ are available. Adding and subtracting $QJ_{R\text{inv}}\dot{x}_r$ to (21), we obtain

$$\hat{S}_q = QJ_{R\text{inv}}S_{vv} - \Gamma_{F_2}J_\varphi^T(q)S_{vF} - Q\Delta J_{R\text{inv}}\dot{x}_r$$
$$= S_q - Q\Delta J_{R\text{inv}}\dot{x}_r \qquad (22)$$

for $\Delta J_{R\text{inv}} = \widehat{J_{R\text{inv}}} - J_{R\text{inv}}$, which arises from the uncalibrated camera.

VI. OPEN-LOOP ERROR EQUATION

Using the uncertainties of nominal references $(\hat{\dot{q}}_r, \hat{\ddot{q}}_r)$ into the parameterization of *Property II* yields

$$H(q)\hat{\ddot{q}}_r + C(q,\dot{q})\hat{\dot{q}}_r + g(q) + J^T(q)B_tJ(q)\hat{\dot{q}}_r = \hat{Y}_r\theta_b$$
$$\qquad (23)$$

where $\hat{\ddot{q}}_r = f(\ddot{x}_r, \ddot{q}_{rf})$, with

$$\ddot{x}_r = \ddot{x}_{vd} - \psi\Delta\dot{x}_v + \dot{S}_{vd} - \Gamma_{v_1}S_{v\delta} - \Gamma_{v_2}\text{sign}(S_{v\delta}) \qquad (24)$$
$$\ddot{q}_{rf} = \Delta\dot{F} - \dot{S}_{Fd} + \Gamma_{F_1}S_{F\delta} + \Gamma_{F_2}\text{sign}(S_{F\delta}) \qquad (25)$$

which introduces discontinuous terms. To avoid introducing high-frequency discontinuous signals, it was decided to add and subtract $\tanh(\mu_v S_{v\delta})$ and $\tanh(\mu_F S_{F\delta})$ to $\hat{\dot{q}}_r$, for $(\mu_v, \mu_F) > 0$, in order to separate continuous and discontinuous signals as follows:

$$\hat{\dot{q}}_r = \hat{\dot{q}}_c + Q\Gamma_{v_2}z_v - J_\varphi^T(q)\Gamma_{F_2}z_F \qquad (26)$$

with $z_v = \tanh(\mu_v S_{v\delta}) - \text{sign}(S_{v\delta})$ and $z_F = \tanh(\mu_F S_{F\delta}) - \text{sign}(S_{F\delta})$.

Therefore, (23) becomes

$$H(q)\hat{\ddot{q}}_r + C(q,\dot{q})\hat{\dot{q}}_r + g(q) + J^T(q)B_tJ(q)\hat{\dot{q}}_r$$
$$= \hat{Y}_c\theta_b + H(Q\Gamma_{v_2}z_v - J_\varphi^T(q)\Gamma_{F_2}z_F). \qquad (27)$$

In this way, $\hat{Y}_c = Y_r(q, \dot{q}, \hat{\dot{q}}_r, \hat{\ddot{q}}_{rc})$ is continuous since $(\hat{\dot{q}}_r, \hat{\ddot{q}}_{rc})$ are continuous, where

$$\hat{\ddot{q}}_{rc} = Q\widehat{J_{R\text{inv}}}\ddot{x}_{rc} + \dot{Q}\widehat{J_{R\text{inv}}}\dot{x}_{rc} + Q\dot{\widehat{J_{R\text{inv}}}}\dot{x}_{rc}$$
$$+ \Gamma_{F_2}J_\varphi^T(q)\ddot{q}_{rc} + \Gamma_{F_2}\dot{J}_\varphi^T(q)\dot{q}_{rc} \qquad (28)$$

with

$$\ddot{x}_{rc} = \ddot{x}_{vd} - \psi\Delta\dot{x}_v + \dot{S}_{vd} - \Gamma_{v_1}S_{v\delta} - \Gamma_{v_2}\tanh(\mu_v S_{v\delta})$$
$$\qquad (29)$$

$$\ddot{q}_{rfc} = \Delta\dot{F} - \dot{S}_{Fd} - \Gamma_{F_1}S_{F\delta} - \Gamma_{F_2}\tanh(\mu_F S_{F\delta}). \qquad (30)$$

Adding and subtracting (27) to (1), we finally obtain the following uncalibrated open-loop error equation

$$H(q)\dot{\hat{S}}_q = \tau - [C(q,\dot{q}) + J^T(q)B_tJ(q)]\hat{S}_q + J_{\varphi+}^T(q)\lambda$$
$$- \hat{Y}_c\theta_b + H\left(Q\Gamma_{v_2}z_v - J_\varphi^T(q)\Gamma_{F_2}z_F\right). \qquad (31)$$

VII. CONTROL DESIGN

Assuming that $(x_v, \dot{x}_v)$ are measurable by the camera, $(q, \dot{q})$ are measurable by the encoder and the tachometer respectively, as well as (λ, F) by a force sensor and the task is designed such that $(x_{vd}, \dot{x}_{vd}) \in \Omega_x$, for $\Omega_x = \{x_v|rank(J_{R\text{inv}}) = 2, \forall x_v\}$, and $\lambda_d(t) = G(\cdot)$, where $G(\cdot)$ is a differentiable function up to the first order, then we have the following theorem.

Theorem 1: Assume that the initial conditions and the desired trajectories belong to $\Omega = [\Omega_q, \Omega_x]$, and consider the robot dynamics (1), (2) in closed loop with the following visual adaptive force-position control law

$$\tau = -K_d\hat{S}_q + \hat{Y}_c\theta_b + J_{\varphi+}^T(q)[-\lambda_d + \eta\Delta F]$$
$$+ \Gamma_{F_2}J_{\varphi+}^T(q)[\tanh(\mu_f S_{F\delta})$$
$$+ \eta\int_{t_0}^t \text{sign}[S_{F\delta}(\zeta)]d\zeta] \qquad (32)$$

$$\dot{\hat{\theta}}_b = -\Gamma\hat{Y}_c^T\hat{S}_q \qquad (33)$$

where $\hat{\theta}_{\mathrm{b}}$ is the online estimation of the constant robot parameter vector, $\eta > 0$ and $\Gamma = \Gamma^T \in \Re_+^{p \times p}$, $K_d = K_d^T \in \Re_+^{2 \times 2}$. If K_d is large enough, the error of initial conditions is small enough, and if

$$\Gamma_{v_2} \geq \left\| \frac{d}{dt} \{ R_J [\hat{S}_q + (\Delta J_{R\mathrm{inv}}) \dot{x}_r] \} \right\|$$

$$\Gamma_{F_2} \geq \left\| \frac{d}{dt} [J_\varphi^\# (q) \hat{S}_q] \right\|$$

with, $R_J = \alpha h(z) R(\theta_v) J(q)$, and $J_\varphi^\#(q) = (-\Gamma_{F_2} J_\varphi(q) J_\varphi^T(q))^{-1} J_\varphi(q)$, then the exponential convergence of visual and force tracking errors is guaranteed.

Proof: The proof is based on the Lyapunov stability criteria, and the second-order sliding modes to finally guarantee local exponential simultaneous tracking of the visual position and the velocities, as well as the contact force. A brief outline of the proof can be stated as follows.

- *Part I*: Boundedness of the closed loop trajectories. In this part, the passivity from the joint velocity error $\hat{S}_q$ input to the torque τ output is established. If the dynamical friction is considered, then the dissipativity is established. This implies that the boundedness of all the closed-loop signals of the closed-loop system is proved.
- *Part II*: Second-order sliding modes. Once the boundedness of the input signals is proved, the regime of the sliding modes for the visual and the force subspaces needs to be induced. Then, the proper gains $\Gamma_{v_2}, \Gamma_{F_2}$, are settled down in this part.
- *Part III*: Exponential convergence of tracking errors. The proper gain selection guarantees the sliding mode for each subspace for all time. Then, we prove that each sliding mode induces the exponential convergence of the visual tracking errors as well as the force tracking errors for all time.

The full details of the proof are given in Appendix A. ∎

Remark 3: Apparently, there is a problem with $J(q(t))^{-1}$ because the visual position converges to the desired visual position exponentially without overshoot, i.e., $x_v(t) \to x_{vd}(t)$, $x_{vd}(t) \in \Omega_x \Rightarrow x_v(t) \in \Omega_x$. However, this is no guarantee that $J(q(t))^{-1}$ is always well posed, because the joint position q converges to the desired joint position q_d with an exponential envelope $q(t) \to q_d(t)$, not with exponential convergence. Thus q may experience a short transient and as a consequence $J(q)$ may loose rank. However, $q(t) \to q_d(t)$ locally, which means that $J(q(t)) \to J(q_d(t))$ within Ω_q. Consequently $J(q(t))^{-1}$ is locally well posed, i.e., $rank(J_\varphi(q(t))^{-1}) = 2, \forall t$. In addition, it is customary that in the visual servoing tasks, the desired trajectories are designed well within Ω_x therefore well within Ω_q, i.e., away from the singular joint configurations.

Remark 4: The continuous function $\tanh(\cdot)$ is used instead of $\mathrm{sign}(\cdot)$ in the control law without jeopardizing the second-order sliding mode, i.e., a signum function is not needed to induce sliding modes in contrast to the first-order sliding modes theory.

Remark 5: The control law is easy to implement and presents low computational cost, even though the proof—however straightforward—is quite involved to follow.

VIII. VISUAL DYNAMIC FRICTION COMPENSATION

Let us consider the joint dynamic friction, which represents a very realistic behavior when the robot is moving along a rigid surface, in particular, driven by visual servoing. In this case, the following *LuGre* [17] dynamic friction model is suitable

$$F(\dot{q}, \dot{\omega}, \omega) = \sigma_0 \omega + \sigma_1 \dot{\omega} + \sigma_2 \dot{q}$$

$$\dot{\omega} = -\sigma_0 k(\dot{q}) \omega + \dot{q},$$

$$k(\dot{q}) = \frac{|\dot{q}|}{\alpha_0 + \alpha_1 e^{-(\dot{q}/\dot{q}_s)^2}} \qquad (34)$$

where the diagonal matrix parameters $(\sigma_1, \sigma_2, \sigma_3) \in \Re_+^{2 \times 2}$, the state $(\omega, \dot{\omega}) \in \Re^2$ stands for the position of the bristles, $(\alpha_0, \alpha_1) > 0$, and $\dot{q}_s \in \Re_+^2$. This model displays outwardly a very complex dynamics around the trivial equilibrium, for the bidirectional motion and for the very small displacements. The forces that come out of this model makes it impossible to reach the origin due to the limit cycles that may induce an unstable behavior. Substituting (34) into (1) yields

$$H(q)\ddot{q} = -C(q, \dot{q})\dot{q} - J(q)^T B_t J(q) \dot{q} + \tau + J_\varphi^T(q)\lambda$$
$$- \sigma_{12} \dot{q} - g(q) - \sigma_0 \omega + \sigma_{01} k(\dot{q}) \omega \qquad (35)$$

where $\sigma_{01} = \sigma_0 \sigma_1$ and $\sigma_{12} = \sigma_1 + \sigma_2$. Now, we need to reorganize the parameterization in terms of two regressors

$$H(q)\ddot{q}_{rc} + [C(q, \dot{q}) + J(q)^T B_t J(q) + \sigma_{12}]\dot{q}_{rc} + g(q) = \hat{Y}_c \theta_b$$

$$\frac{\sigma_{01}\alpha_{01}}{\alpha_0} |\dot{q}| \tanh(\xi_f \hat{S}_q) + \sigma_0 \alpha_{01} \tanh(\xi_f \hat{S}_q) = \hat{Y}_f \theta_f$$

where $\hat{Y}_f \theta_f$ stands as a virtual *continuous* regressor, with $\alpha_{01} = \alpha_0 + \alpha_1$, and $\xi_f > 0$. Now adding and subtracting the above regressors to (35) yields the following uncalibrated open-loop error dynamics with dynamic friction

$$H(q)\hat{S}_q = -[C(q, \dot{q}) + J(q)^T B_t J(q) + \sigma_{12}]\hat{S}_q$$
$$+ \tau - F - Y\Theta + J_{\varphi+}^T(q)\lambda + \sigma_{01} k(\dot{q}) \omega$$
$$- \sigma_0 \omega + H(Q\Gamma_{v_2} z_v - J_\varphi^T(q)\Gamma_{F_2} z_F) \qquad (36)$$

with

$$F = \sigma_0 \left\{ \omega + \left(\alpha_{01} + \alpha_0^{-1} \sigma_1 \alpha_{01} |\dot{q}| \right) \tanh(\xi_f \hat{S}_q) \right.$$

$$\left. + \sigma_1 |\dot{q}| \omega \left(\alpha_0 + \alpha_1 e^{-(\dot{q}/\dot{q}_s)^2} \right)^{-1} \right\}$$

where $Y = [\hat{Y}_c, \hat{Y}_f]$ and $\Theta = [\theta_b^T, \theta_f^T]^T$. Finally, consider the following control law

$$\tau = -K_d \hat{S}_q + Y\hat{\Theta} + J_{\varphi+}^T(q)[-\lambda_d + \eta \Delta F]$$

$$+ \Gamma_{F_2} J_{\varphi+}^T(q) \left[\tanh(\mu_f S_{F\delta}) + \eta \int_{t_0}^t \mathrm{sign}[S_{F\delta}(\zeta)] d\zeta \right]$$
$$\qquad (37)$$

$$\dot{\hat{\Theta}} = -\Gamma Y^T \hat{S}_q \qquad (38)$$

with $\hat{\Theta}$ as an estimation of Θ, where $\eta>0$ and $\Gamma \in \Re_+^{p \times p}$, $K_d \in \Re_+^{2 \times 2}$. We now have the following result.

Theorem 2: Assume that the initial conditions and the desired trajectories belong to $\Omega = [\Omega_q, \Omega_x]$, and consider the controller (37), (38). If K_d is large enough and the error of the initial conditions is small enough, and if

$$\Gamma_v \geq \left\| \frac{d}{dt}\{R_J[\hat{S}_q + (\Delta J_{R\text{inv}})\dot{x}_r]\} \right\|$$

$$\Gamma_{F_2} \geq \left\| \frac{d}{dt}[J_\varphi^\#(q)\hat{S}_q] \right\|$$

then the exponential convergence of the visual and the force tracking errors is guaranteed.

Proof: The proof is based on Lyapunov stability criteria, as in the Theorem 1. Full details of the proof are given in Appendix B. ∎

Remark 6: Theorem 2 yields an image-based dynamical control scheme for the constrained robots that fuses the visual, the encoder and the force signals with the compensation of dynamic friction by means of the *visual feedback*.

Remark 7: When no friction is considered at all, Theorems 1 and 2 deliver similar control structures, however with less conservative stability domains and with smaller feedback control gains.

Remark 8: Joint friction compensation schemes, e.g., [17], [19], and [20], which are based on joint errors, are faster and accurate in comparison to visual (*image based*) friction compensation, because typically the joint sensor attains higher resolution than the camera. However, it is not possible to implement the joint friction compensation into an uncalibrated image-based controller because: 1) joint errors are not available in an uncalibrated visual servoing scheme and 2) passivity inequality of a feedback system is established for an unique pair of torque input to error output [21]. Therefore, it cannot be introduced as an inner joint friction control loop with one output signal and an outer visual friction control loop with another output signal for a unique energy storage function.

IX. EXPERIMENTAL STATION

A planar robot system is integrated (see Fig. 2). The robot parameters and the camera parameters are shown in Tables I and II, respectively. Control feedback gains and dynamic friction parameters are depicted in Tables III and IV, respectively.

A. Hardware

Direct-drive Yaskawa ac servomotors SGM-08A314 and SGM-04U3B4L with 2048 pulse encoders are directly coupled to the links of the 2-DOF arm. Digital drives Yaskawa servopacks (SGD-08AS and SGDA-04AS) are integrated. A six-axes force-moment sensor 67M25A-I40-200N12 by JR3 Inc., provided with a DSP- based interface system for the PCI bus is mounted at the end effector of the robot. A rigid aluminum 6101 probe with a bearing SKF R8-2Z in its tip is attached at the end-deffector to validate only the contact viscous friction, as shown in Fig. 2. The robot task is to move its tool-tip along a specified
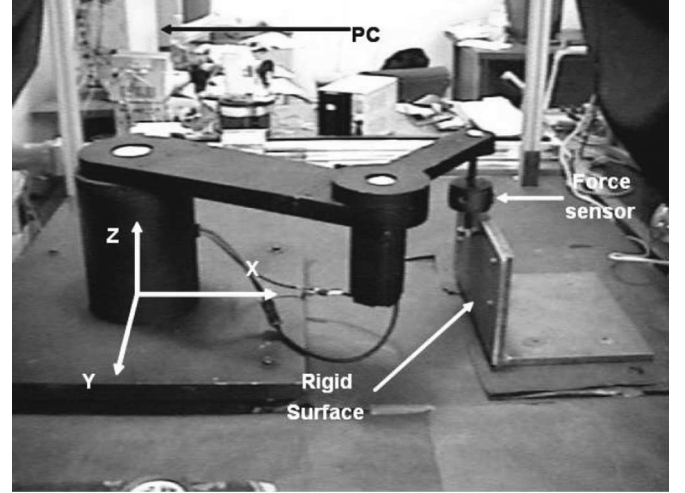
Fig. 2. Experimental setup.

TABLE I
ROBOT PARAMETERS

	Mass	Length	Center of Mass	Inertia
Link 1	7.1956 Kg	0.4 m	0.1775 m	0.2779 Kg m²
Link 2	1.8941 Kg	0.3 m	0.0979 m	0.0239 Kg m²

TABLE II
CAMERA PARAMETERS

Parameter	Value
Rotation angle θ_v	90°
Scale factor α	99500 pix/m
Depth field of view z	1.6 m
Camera offset β	$[-335\ -218]^T$ pix
Focal length λ_v	0.08 m

TABLE III
FEEDBACK GAINS

Gain	Value	Gain	Value	Gain	Value
K_d	*diag*(14,1.8)	Ψ	*diag*(5,5)	$\Gamma_{v(1,2)}$	*diag*(8,8)
κ_v	20	κ_F	20	β_t	2
$\Gamma_{F(1,2)}$	*diag*(3,3)	Γ	1	η	2.8

TABLE IV
DYNAMIC FRICTION PARAMETERS

Parameter	Value	Parameter	Value
σ_0	diag(30000, 10000)	α_0	diag(3,1)
σ_1	diag(2,1)	α_1	diag(0.4 0.2)
σ_2	diag(2,1)	$\dot{q}_s$	diag(0.01,0.005)

trajectory over the steel surface while exerting a specified profile of force normal to the surface. A fixed SONY DFW-V500 CCD camera was used. The robot is initialized with a high-gain PD. The inertial frame of the whole system is at the base of the robot and the contact surface is at $y = 136$ *pixel* rendering a XZ plane.
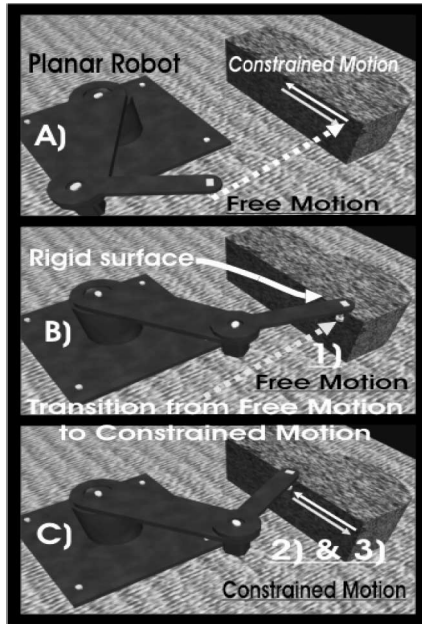
Fig. 3. Experimental phases. (a) Free motion and constrained motion. (b) Free motion. (c) Constrained motion.

B. Software

A 2.2-GHz personal computer (PC), running on the Debian GNU/Linux 3.1 "Sarge" (kernel 2.4-27) with the RTAI patch operating system (RTAI 3.1.0-4) is used. This PC implements two real-time concurrent processes. The first one sets communication with the SONY DFW-V500 camera via IEEE1394 protocol and controls the acquisition of the robot end-effector position in the image space, with a sampling rate of 30 Hz. The second process, computes the torque output for the servopacks and runs with a sampling rate of 1 kHz. Communication between processes is done by shared memory allocation. Low-level programming provides the interface to a Sensoray 626 I/O card, which contains: an internal analog quadrature encoder interface, 14-b analog resolution outputs, and digital I/O ports. This data acquisition card is used to communicate with the Yaskawa servopacks. Special Linux drivers provide interface to a JR3 DSP-based force sensor receiver used to communicate with the JR3 6DOF force sensor. Velocity is computed using a dirty Euler numerical differentiation formula filtered with a low-pass second-order Butterworth filter, with a cutoff frequency of 20 Hz.

C. Task

In Fig. 3(a), all the experimental faces are depicted (free motion and constrained motion). The experiment is performed as follows.

1) From $t = [0\ 3]$ s [see Fig. 3(b)], the end effector is requested to move, in free motion, from its initial condition until it makes contact with the surface. The end effector lasts 2 s to establish stable contact.

2) From $t = [5\ 8]$ s [see Fig. 3(c)], the tool tip exerts a desired profile of force normal to the surface (0–5 N)
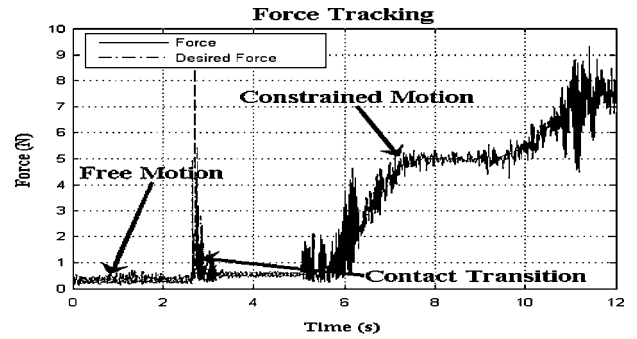
Fig. 4. Force tracking. Different stages of the experiment are depicted.
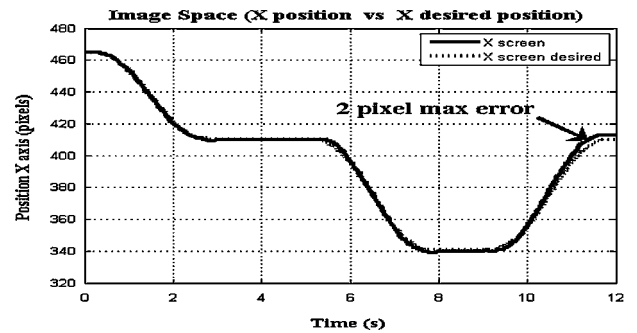
Fig. 5. End-effector tracking in image space (pixels), "X" axis.
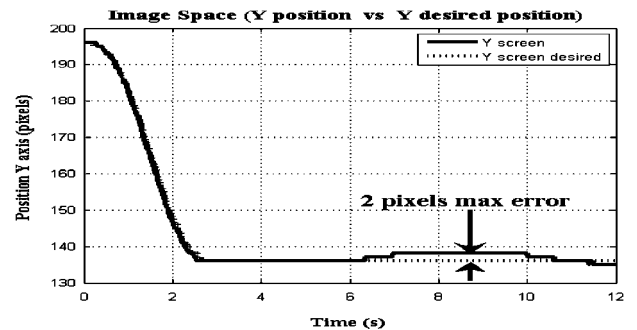
Fig. 6. End-effector tracking in image space (pixels), "Y" axis.

while moving forward, along X axis, from 410 to 341 pixels.

3) From $t = [8\ 12]$ s [see Fig. 3(c)], the exerted force is incremented (5–7.5 N), while moving backward, along X axis, from 341 to 410 pixels, as can be seen in Figs. 4–6.

Both the desired position and the force are designed with $\Phi(t) = P(t_i) = [X_F - X_i] + X_i$, where $P(t)$ is a fifth-order polynomial that satisfies $P(t_i) = 0, P(t_f) = 1,$ and $\dot{P}(t_i) = \dot{P}(t_f) = 0$. The subscripts "$i$" and "$f$" denote the initial and the final stages, respectively. At the first stage of the experiment, the control law (37)–(38) is used with the force part set to zero, i.e., $J_\varphi^T(q) = 0$ and $Q = I$. In [7] and [8], it is proved that this scheme is stable for unconstrained motion. Once the tool-tip
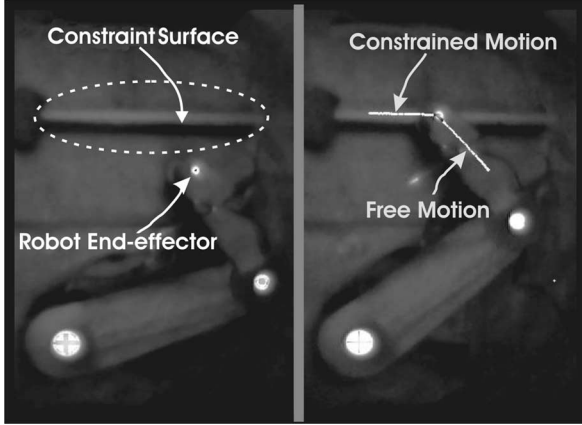
Fig. 7. Camera point of view of the robot task. The white marks are the on-line visual tracking of the robot end-effector.
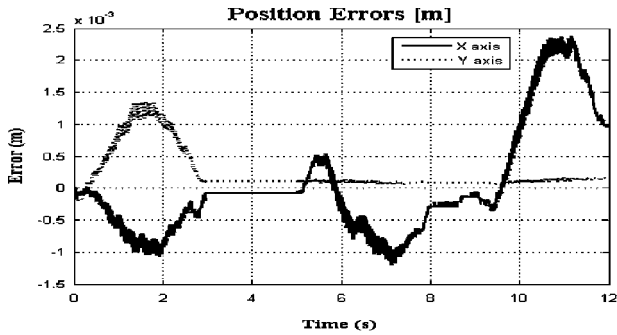
Fig. 8. Cartesian robot task errors (m).

is in stable contact with the surface, the control force term is switched on.

X. RESULTS

Fig. 9 shows the joint torques. It can be observed that the control output without saturation is obtained. The torque noise present in the free motion segment shown in Fig. 9 occurs because the control gains are tuned for position-force control task, i.e., these are high gains for a simple free motion, which causes the very high response of the system. Fig. 8 depicts the tracking errors in the Cartesian robot space (m). The seemingly high frequency is because this task requires very precise control, but the sensor resolution is limited to 1 pixel and JR3 force sensor noise is $\pm 2N$.[8] In Fig. 4, the exerted force profile is shown. As can be seen, from [1 3] s the robot end effector performs free motion (near to $0N$) until it makes contact with the surface (an overshoot in the contact force is presented due to contact transition), then it remains in that state for two more seconds and from [5 8] s, increases the applied force smoothly from [0 5]N, while it moves forward over the x axis, and finally from [8 12] s once again increases the exerted force [5 7.5] N, while it moves backward. The noisy signal is caused by the high precision of

[8]Better plots can easily be obtained simply by reducing the desired visual velocity, increasing $\lambda_d(t)$ or using subpixel resolution.
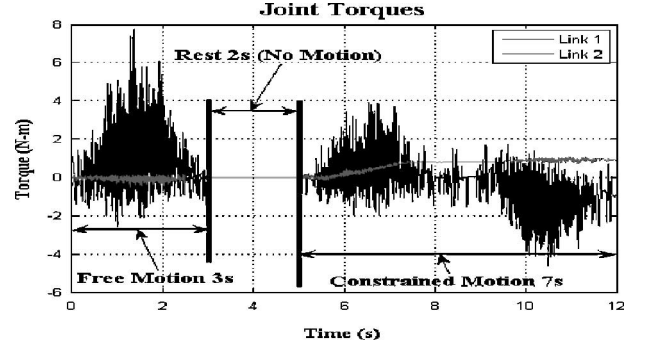
Fig. 9. Joint torques without saturation. Better plots can easily be obtained simply reducing the desired visual velocity or increasing $\lambda_d(t)$.

the JR3 sensor. In Figs. 5 and 6, the robot end-effector motion in the image space (pixels) is shown, the image-coordinated system is rotated by θ_v degrees (in this case $90°$), the maximum error is 2 pixels, and the performance of the robot (see Fig. 7) can be improved using subpixel resolution.

A. Conclusion

A novel scheme for adaptive image-based visual servoing of the constrained dynamical planar robots under friction is proposed. The main feature is the ability to fuse *uncalibrated image coordinates* into an orthogonal complement of joint velocities, and *integral of contact forces*. This allows to yield *exponential convergence* for image-based position velocity and contact forces even when the robot parameters, the camera parameters, and the contact viscous friction are considered unknown. Additionally, a compensator of uncertain joint dynamic friction is presented, which is usually neglected in visual servoing, but it is of particularly concern in visual motion tasks because the motion regime is slow with velocity reversals. Experimental results comply with the theoretical stability properties.

APPENDIX A

PROOF OF THEOREM 1

The closed-loop dynamics between (32), (33), and (31) yields

$$H(q)\dot{\hat{S}}_q = -\{K_d + C(q,\dot{q})\}\hat{S}_q - \hat{Y}_c\Delta\theta_b$$
$$+ J_{\varphi+}^T(q)[\Delta\lambda + \Gamma_{F_2}\tanh(\mu_F S_{F\delta})]$$
$$+ \eta J_{\varphi+}^T(q)[\Delta F + \Gamma_{F_2}\int_{t_0}^t \text{sign}[S_{F\delta}(\zeta)]\,d\zeta]$$
(39)

$$\Delta\dot{\theta}_b = \Gamma\hat{Y}_c^T\hat{S}_q \tag{40}$$

with $\Delta\theta_b = \theta_b - \hat{\theta}_b$. The proof is organized in three parts.

Part I: Boundedness of closed-loop trajectories. Consider the time derivative of the following *Lyapunov* candidate function

$$V = \frac{1}{2}\left[\hat{S}_q^T H(q)\hat{S}_q + \Gamma_{F_2}S_{vF}^T S_{vF} + \Delta\theta_b^T\Gamma^{-1}\Delta\theta_b\right]$$
(41)

along the solutions of (39)–(40) as

$$\dot{V} \leq -K_d \|\hat{S}_q\|_2^2 - \eta \Gamma_{F_2} \|S_{vF}\| + \|\hat{S}_q\| \psi \qquad (42)$$

where *Property I* has been used, ψ is a functional depending on the state and error manifolds, similar to [22]. Now if K_d and Γ_{F_2} are large enough and errors of initial conditions are small enough, we conclude the seminegative definiteness of (42) outside of the hyperball $\varepsilon_0 = \{\hat{S}_q \mid \dot{V} < 0\}$ centered at the origin, such that the following properties of the state of closed-loop system arise

$$(\hat{S}_q, S_{vF}) \in L_\infty \rightarrow (\|S_{vv}\|, \|S_{vF}\|) \in L_\infty. \qquad (43)$$

Then, $(S_{v\delta}, \int_{t_0}^t \operatorname{sign}[S_{v\delta}(\zeta)] \, d\zeta) \in L_\infty$ and since the desired trajectories are differentiable functions and feedback gains are bounded, we have that $(\hat{\dot{q}}_r, \hat{\ddot{q}}_r) \in L_\infty$. The right-hand side of (39) shows that there exists $\varepsilon_1 > 0$ such that $\|\hat{\dot{S}}_q\| \leq \varepsilon_1$. This result shows only the local stability of $(\hat{S}_q, \hat{\dot{S}}_q)$. Now we prove that the sliding modes arise. Rewriting (22) in terms of two orthogonal vectors, we obtain

$$\hat{S}_q = Q\{J_{R\text{inv}} S_{vv} - \Delta J_{R\text{inv}} \dot{x}_r\} - J_\varphi^T(q)\{\Gamma_{F_2} S_{vF}\}. \qquad (44)$$

Since $\hat{S}_q \in L_2$, and $J_{R\text{inv}}$ and Q are bounded, then $QJ_{R\text{inv}} S_{vv}$ is bounded and as $\varphi(q)$ is smooth and lies in the reachable robot space and $S_{vF} \rightarrow 0$, then $J_\varphi^T(q)\Gamma_{F_2} S_{vF} \rightarrow 0$. Now, taking into account that $\hat{\dot{S}}_q$ is bounded, then $\frac{d}{dt}(J_{R\text{inv}} Q S_{vv})$ and $\frac{d}{dt}(J_\varphi^T(q)\Gamma_{F_2} S_{vF})$ are bounded [this is possible because $(\dot{J}_\varphi^T(q), \dot{Q})$ are bounded]. All this chain of conclusions prove that there exist constants $\varepsilon_2 > 0$ and $\varepsilon_3 > 0$ such that $|\dot{S}_{vv}| < \varepsilon_2, |\dot{S}_{vF}| < \varepsilon_3$.

Now we have to prove that for a proper selection of feedback gains Γ_{v_2} and Γ_{F_2}, the trajectories of visual position and force converge to zero. This is possible if we can prove that the sliding modes are established in the visual subspace Q and in the force subspace $J_\varphi^T(q)$. Considering that operators $QJ_{R\text{inv}}$ and $J_\varphi^T(q)\Gamma_{F_2}$ span the vector $\hat{S}_q$ as the direct sum of its image $im\{QJ_{R\text{inv}}(S_{vv})\} \equiv S_{vv}^{im}$ and $im\{J_\varphi^T(q)\Gamma_{F_2}(S_{vF})\} \equiv S_{vF}^{im}$, respectively [see (44)]. This implies that

$$\hat{S}_q = Q\{J_{R\text{inv}} S_{vv} - \Delta J_{R\text{inv}} \dot{x}_r\} - J_\varphi^T(q)\{\Gamma_{F_2} S_{vF}\}$$
$$= (S_{vv}^{im} - im\{\Delta J_{R\text{inv}}\}) - S_{vF}^{im} \qquad (45)$$

where $S_{vv}^{im} - im\{\Delta J_{R\text{inv}}\}$ and S_{vF}^{im} belong to orthogonal complements, thus, S_{vF}^{im} belongs to the kernel of Q. This is verified if we multiply (45) by Q^T, i.e.,

$$Q^T \hat{S}_q = Q^T Q\{J_{R\text{inv}} S_{vv} - \Delta J_{R\text{inv}} \dot{x}_r\} - \underbrace{Q^T J_\varphi^T(q)\Gamma_{F_2} S_{vF}}_{zero}$$
$$= S_{vv}^{im} - im\{\Delta J_{R\text{inv}} \dot{x}_r\} \qquad (46)$$

since Q is idempotent. It is important to notice that if $Ax = Ay$ for any square nonsingular matrix A and any couple of vectors x, y, then $x \equiv y$. Thus, (46) means that the image subspace $\hat{S}_q = Q\{J_{R\text{inv}} S_{vv} - \Delta J_{R\text{inv}} \dot{x}_r\}$ is valid within span Q. Now

if we multiply $\hat{S}_q$ by $J_\varphi^\#(q)$, we obtain

$$J_\varphi^\#(q)\hat{S}_q = \underbrace{J_\varphi^\#(q)Q\{J_{R\text{inv}} S_{vv} - \Delta J_{R\text{inv}} \dot{x}_r\}}_{zero}$$
$$\qquad\qquad - \Gamma_{F_2} J_\varphi^\#(q) J_\varphi^T(q) S_{vF}$$
$$J_\varphi^\#(q)\hat{S}_q = S_{vF} \qquad (47)$$

which is the force subspace, orthogonal to (46).

Part II: Second-order sliding modes.

Part II.a: Sliding modes for the velocity subspace. According to (46), we have

$$Q^T \hat{S}_q = Q\{J_{R\text{inv}} S_{vv} - \Delta J_{R\text{inv}} \dot{x}_r\}$$

then

$$\hat{S}_q \equiv J_{R\text{inv}} S_{vv} - \Delta J_{R\text{inv}} \dot{x}_r \qquad (48)$$

in the image subspace of Q. However, notice that when Q is not full rank, then this equivalence is valid locally, not globally. In this local neighborhood, if we multiply (48) by R_J,[9] we have

$$R_J \hat{S}_q = S_{v\delta} + \Gamma_{v_1} \int_{t_0}^t S_{v\delta}(\zeta) \, d\zeta + \Gamma_{v_2} \int_{t_0}^t \operatorname{sign}[S_{v\delta}(\zeta)] \, d\zeta$$
$$\qquad - R_J\{\Delta J_{R\text{inv}} \dot{x}_r\} \qquad (49)$$

Taking the time derivative of (49), and multiplying it by $S_{v\delta}^T$, it produces

$$S_{v\delta}^T \dot{S}_{v\delta} = -\Gamma_{v_2} S_{v\delta}^T \operatorname{sign}(S_{v\delta}) - \Gamma_{v_1} S_{v\delta}^T S_{v\delta}$$
$$\qquad + S_{v\delta}^T \frac{d}{dt}[R_J(\hat{S}_q + \Delta J_{R\text{inv}} \dot{x}_r)]$$
$$\qquad \leq -\mu_v |S_{v\delta}| - \Gamma_{v_1} \|S_{v\delta}\|_2^2$$

where $\varepsilon_4 \geq |\frac{d}{dt}[R_J(\hat{S}_q + \Delta J_{R\text{inv}} \dot{x}_r)]|$, and $\mu_v = \Gamma_{v_2} - \varepsilon_4$. Thus, we obtain the sliding condition if $\Gamma_{v_2} > \varepsilon_4$. This guarantees the sliding mode at $S_{v\delta} = 0$ at $t_v = \frac{|S_{v\delta}(t_0)|}{\mu_v}$. However, notice that for any initial condition $S_{v\delta}(t_0) = 0$, then $t_v = 0$, which implies that the sliding mode at $S_{v\delta}(t) = 0$ is guaranteed for all time.

Part II.b: Sliding modes for the force subspace. Equation (47) leads to

$$J_\varphi^\#(q)\hat{S}_q = S_{F\delta} + \Gamma_{F_1} \int_{t_0}^t S_{F\delta}(\zeta) \, d\zeta$$
$$\qquad + \Gamma_{F_2} \int_{t_0}^t \operatorname{sign}[S_{F\delta}(\zeta)] \, d\zeta \qquad (50)$$

Taking the time derivative of (50) and multiplying it by $S_{F\delta}^T$, (50) becomes

$$S_{F\delta}^T \dot{S}_{F\delta} \leq -\Gamma_{F_1} \|S_{F\delta}\|_2^2 - \Gamma_{F_2} |S_{F\delta}| + |S_{F\delta}| \frac{d}{dt}(J_\varphi^\#(q)\hat{S}_q)$$
$$\qquad \leq -\mu_F |S_{F\delta}| - \Gamma_{F_1} \|S_{F\delta}\|_2^2$$

---

[9]Remember the equality $[J_{R\text{inv}} = J(q)^{-1} R(\theta_v)^{-1} h(z)^{-1} \alpha^{-1}$.

where $\varepsilon_5 \geq |\frac{d}{dt}[J_\varphi^{\#}(q)\hat{S}_q]|$ and $\mu_F = \Gamma_{F_2} - \varepsilon_5$. If $\Gamma_{F_2} > \varepsilon_5$, then a sliding mode at $S_{v\delta} = 0$ is induced at $t_F = \frac{|S_{F\delta}(t_0)|}{\mu_F}$, but $S_{F\delta}(t_0) = 0$, thus $S_{F\delta}(t) = 0$ is guaranteed for all time.

Part III: Exponential convergence of tracking errors.

Part III.a: Visual tracking errors. Since a sliding mode exists for all time at $S_{v\delta}(t) = 0$, then we have

$$S_v = S_{vd} \forall t \rightarrow \Delta\dot{x}_v = -\Psi\Delta x_v + S_v(t_0)e^{-\kappa_v t}\forall t$$

which implies that the visual tracking errors locally tend to zero exponentially fast, i.e., $x_v \rightarrow x_{vd}$, $\dot{x}_v \rightarrow \dot{x}_{vd}$, implying that the robot end effector converges to the desired image x_{vd}, with given velocity $\dot{x}_{vd}$. ∎

Part III.b: Force tracking errors. Since a sliding mode at $S_{F\delta}(t) = 0$ is induced for all time, this means that $\Delta F = \Delta F(t_0) e^{-\kappa_F t}$. Moreover, in [22], it is shown that the convergence of force tracking errors arises, thus $\lambda \rightarrow \lambda_d$ exponentially fast. ∎

APPENDIX B

PROOF OF THEOREM 2

With the very same Lyapunov function of *Theorem 1*, we obtain the following time derivative, along trajectories of the closed loop of (37), (38), and (36)

$$\dot{V} \leq -K_d\|\hat{S}_q\|_2^2 - \eta\Gamma_{F_2}\|S_{vF}\| + \|\hat{S}_q\|\psi - \dot{V}_f \qquad (51)$$

where

$$\dot{V}_f = \sigma_0\hat{S}_q^T[\omega + \sigma_{01}\tanh(\xi_f\hat{S}_q)]$$
$$- \sigma_{01}\hat{S}_q[-\omega k(\dot{q}) + \alpha_0^{-1}\alpha_{01}|\dot{q}|\tanh(\xi_f\hat{S}_q)].$$

In [20], we proved that $\dot{V}_f > 0$, and $|\dot{V}_f| < \varepsilon_6$, $\varepsilon_6 > 0$. Then, $\dot{V}_f$ is positive definite outside the hyperball $\rho_0 = \rho_0(\hat{S}_q) = \{\hat{S}_q|V_f \leq 0\}$ with $\|\rho_0\| \leq \rho$, for $\rho > 0$. Then, (55) becomes

$$\dot{V} \leq -K_d\|\hat{S}_q\|_2^2 - \eta\Gamma_{F_2}\|S_{vF}\| + \|\hat{S}_q\|\psi + \rho_0. \qquad (52)$$

Afterwards, we proceed similar to proof of Theorem 1, and it is therefore omitted.

ACKNOWLEDGMENT

The authors thank all the reviewers for their time, interesting comments, and/or useful corrections.

REFERENCES

[1] S. Arimoto, Y. H. Liu, and T. Naniwa, "Model based adaptive hybrid control for geometrically constrained robot manipulator," in *Proc. IEEE Int. Conf. Robot. Autom.*, 1993, pp. 618–623.

[2] F. Miyazaki and Y. Masutani, "Robustness on sensory feedback control based on imperfect jacobian," in *Proc. Robotics Research: Fifth Int. Symp.* H. Miura and S. Arimoto, Eds. Cambridge, MA: MIT, 1990, pp. 201–208.

[3] B. E. Bishop and M. W. Spong, "Adaptive calibration and control of 2D monocular visual servo system," in *Proc. IFAC Symp. Robot. Control*, Nantes, France, 1997, pp. 525–530.

[4] R. Kelly and A. Marquez, "Fixed-eye direct visual feedback control of planar robots," *J. Syst. Eng.*, vol. 4, no. 5, pp. 239–248, Nov. 1995.

[5] R. Kelly, "Robust asymptotically stable visual servoing of planar robots," *IEEE Trans. Robot. Autom.*, vol. 12, no. 5, pp. 759–766, Oct. 1996.

[6] E. Zergeroglu, D. M. Dawson, M. S. de Queiroz, and P. Setlur, "Robust visual-servo control of robot manipulators in the presence of uncertainty," *J. Robot. Syst.*, vol. 20, no. 2, pp. 93–106, 2003.

[7] E. C. Dean-León, V. Parra-Vega, A. Espinosa-Romero, and J. Fierro, "Dynamical image-based PID uncalibrated visual servoing with fixed camera for tracking of planar robots with a heuristical predictor," in *Proc. 2nd IEEE Int. Conf. Ind. Info.*, 2004, pp. 339–345.

[8] L. G. García, E. C. Dean-León, V. Parra-Vega, A. Espinosa-Romero, and J. Fierro, "Experimental results of image-based adaptive visual servoing of 2D robots under jacobian and dynamic friction uncertainties," presented at the Int. Symp. Computational Intell. Robot. Autom., Espoo, Finland, 2005.

[9] H. Hemami and B. Wyman, "Modeling and control of constrained dynamic system with application to biped locomotion in the frontal plane," *IEEE Trans. Autom. Control*, vol. AC-24, no. 4, pp. 526–535, Aug. 1979.

[10] N. H. McClamroch and D. Wang, "Position and force control for constrained manipulator motion: Lyapunov's direct method," *IEEE Trans. Robot. Autom.*, vol. 9, no. 3, pp. 308–313, Jun. 1993.

[11] D. E. Whitney, "Historical perspective and state of the art in robot manipulators," in *Proc. IEEE Int. Conf. Robot. Autom.*, 1985, pp. 262–268.

[12] O. Kathib, "A unified approach for motion and force control of robot manipulators: The operational space formulation," *IEEE Trans. Robot. Autom.*, vol. RA-3, no. 1, pp. 43–53, Feb. 1987.

[13] A. Namiki, Y. Nakabo, I. Ishii, and M. Ishikawa, "High speed grasping using visual and force feedback," in *Proc. IEEE Int. Conf. Robot. Autom.*, Detroit, MI, 1999, pp. 3195–3200.

[14] S. Jorg, J. Langwald, and M. Nickl, "Flexible robot assembly using a multi-sensory approach," in *Proc. ICRA' 00 IEEE Int. Conf. Robot. Autom.*, 2000, vol. 4, pp. 3687–3694.

[15] K. Hosoda, K. Igarashi, and M. Asada, "Adaptive hybrid control for visual and force servoing in an unknown environment," *IEEE Robot. Autom. Mag.*, vol. 5, no. 4, pp. 39–43, Dec. 1998.

[16] D. Xiao, "Sensor-hybrid position/force control of a robot manipulator in an uncalibrated environment," *IEEE Trans. Control Syst. Technol.*, vol. 8, no. 4, pp. 635–645, Jul. 2000.

[17] C. Canudas de Wit, H. Olsson, and K. J. Astrom, "A new model for control of systems with friction," *IEEE Trans. Autom. Control*, vol. 40, no. 3, pp. 419–425, Mar. 1995.

[18] S. Hutchinson, G. Hager, and P. Corke, "A tutorial on visual servo control," *IEEE Trans. Robot. Autom.*, vol. 12, no. 5, pp. 651–670, Oct. 1996.

[19] E. Panteley, R. Ortega, and M. Gafvert, "An adaptive friction compensator for global tracking in robot manipulators," *Syst. Control Lett.*, vol. 33, no. 5, pp. 307–313, 1998.

[20] V. Parra-Vega, "Adaptive compensation of dynamic friction in finite time of 1 DOF mechanical system," in *Proc. Amer. Control Conf. 25–27*, 2001, vol. 3, pp. 2462–2467.

[21] M. Vidyasagar, *Nonlinear Systems Analysis*, 2nd ed. Englewood Cliffs, NJ: Prentice-Hall.

[22] V. Parra-Vega, S. Arimoto, Yun-Hui Liu, G. Hirzinger, and P. Akella, "Dynamic sliding PID control for tracking of robot manipulators: Theory and experiments," *IEEE Trans. Robot. Autom.*, vol. 19, no. 6, pp. 967–976, Dec. 2003.

Emmanuel C. Dean-León received the B.Eng. degree in industrial robotics from the Escuela Superior de Ingeniería Mecánica y Eléctrica, México D.F., México, in 2000, and the M.Sc. degree in electrical engineering from the Research Center for Advanced Studies (CINVESTAV), San Pedro Zacatenco, México D.F., in 2003. Currently, he is pursuing the Ph.D. degree in electrical engineering at the CINVESTAV.

His current research interests include collaborative multirobots, control theory, visual servoing, computer vision, and robotics.

Vicente Parra-Vega (S'92–M'95) received the B.Eng. degree in control and computing and the B.Eng. degree in electronics and communications, both from the Nuevó Leon University, Nuevó Leon, México, in 1987, the M.Sc. degree in automatic control from the Research Center for Advanced Studies (CINVESTAV), San Pedro Zacatenco, México, in 1989, and the Ph.D. degree in electrical engineering from the Mathematical Engineering and Information Physics Department of the University of Tokyo, Tokyo, Japan in 1995, under the supervision of Prof. S. Arimoto.

He was a Postdoctoral Fellow in the Robotics and Mechatronics Department of the DLR, Wessling, Germany, under the supervision of Prof. G Hirzinger. Currently, he is a Full Professor at the CINVESTAV. His current research interests include collaborative multirobots, high-precision servosystems, haptic interfaces, control theory, visual servoing, teleoperators, high-speed CNC, and unmanned aerial and submarine robots. He is the leading cofounder of two new postgraduate programmes in Mexico, the first one in Mechatronics and the second one in Robotics and Advanced Manufacturing.

Prof. Parra-Vega is a Regular Member of the Mexican Academy of Science, the National Researcher System, and from 1997, he has participated in several committees of the Mexican Council for Science and Technology.

Arturo Espinosa-Romero received the B.Eng. degree in electronics systems from the Tecnológico de Monterrey, Monterrey, México, in 1992 and the Ph.D. degree in informatics from the University of Edinburgh, in 2001.

After his Ph.D., he was a Postdoctoral Fellow at the Institute of Research in Applied Mathematics and Systems of the National Autonomous University of México, México City. Currently, he is a Lecturer and Researcher at the Faculty of Mathematics of the Autonomous University of Yucatan, Yucatan, Mexico. His current research interests include computer vision, robotics, artificial intelligence, and pattern recognition. Presently, he is working on geometrical computer vision for scene reconstruction.